ARTICLES
https://doi.org/10.1038/s41557-021-00661-x

nature chemistry

Cellular uptake of large biomolecules enabled by cell-surface-reactive cell-penetrating peptide additives

Anselm F. L. Schneider[1,2], Marina Kithil[3], M. Cristina Cardoso[3], Martin Lehmann[1] and Christian P. R. Hackenberger[1,4]✉

Enabling the cellular delivery and cytosolic bioavailability of functional proteins constitutes a major challenge for the life sciences. Here we demonstrate that thiol-reactive arginine-rich peptide additives can enhance the cellular uptake of protein–CPP conjugates in a non-endocytic mode, even at low micromolar concentration. We show that such thiol- or HaloTag-reactive additives can result in covalently anchored CPPs on the cell surface, which are highly effective at co-delivering protein cargoes. Taking advantage of the thiol reactivity of our most effective CPP additive, we show that Cys-containing proteins can be readily delivered into the cytosol by simple co-addition of a slight excess of this CPP. Furthermore, we demonstrate the application of our 'CPP-additive technique' in the delivery of functional enzymes, nanobodies and full-length immunoglobulin-G antibodies. This new cellular uptake protocol greatly simplifies both the accessibility and efficiency of protein and antibody delivery, with minimal chemical or genetic engineering.

Proteins offer a tremendous structural and functional diversity, which makes them indispensable tools for biological and pharmacological applications. However, proteins are large and hydrophilic, and thus usually not cell-permeable, which severely limits their potential in both research and therapy. Consequently, the intracellular delivery of functional proteins remains one of the biggest challenges in the molecular life sciences, although considerable progress has been made recently[1,2]. Among other methods, cell-penetrating peptides (CPPs) have established themselves as potent tools in the delivery of a variety of cargoes[3].

The first CPPs or 'protein transduction domains' (PTDs), discovered about 30 years ago, originated from the transactivator of transcription (TAT) protein of the human immunodeficiency virus (HIV)[4] and the *Drosophila* antennapedia homeodomain (penetratin)[5,6]. Since then, many CPPs have been described, with both natural and synthetic origins. Several studies have investigated their mechanisms of action and used them in various applications of biology[7,8]. However, how, exactly, CPPs enter cells remains the subject of controversy. Much effort has been devoted to cationic CPPs, which can bind to cell membranes through ionic interactions before being endocytosed[9,10]. Equally, many reports describe CPP-mediated uptake at cold temperatures, where active uptake processes should not occur, or in the presence of endocytosis inhibitors[11,12]. The latter process, commonly referred to as 'transduction', is reported to be dependent on concentration[13,14] and also on the cargo attached to the peptide[15]. This can be seen when using linear CPPs to transport small cargoes such as fluorophores and peptides, which typically leads to localization in the cytosol, whereas larger protein cargoes are often trapped in endosomes[16,17].

To further improve the delivery of CPP-linked cargoes, researchers have implemented additional modules into uptake protocols. For example, addition of the enzyme sphingomyelinase was found to result in increased uptake of cationic CPPs by generating ceramide on the cell surface[18], while the addition of pyrenebutyrate as a hydrophobic counterion to cells before adding the CPP conjugate led to improved uptake[19]. Finally, the addition of peptides or small molecules has been pursued to mediate endosomal leakage for the release of cargoes into the cytosol[20–24].

An important element in the design of effective CPPs for the transport of cargo to the cytosol is cyclization[25,26]. It has been demonstrated that cyclization leads to a remarkable increase in both the efficiency and speed of membrane transduction[27], probably stemming from the presentation of the positive charges on the peptide. We have previously shown that cyclization and subsequent conjugation of a single TAT peptide can be used to transport green fluorescent protein (GFP) into the cytosol of cells, which was impossible with the linear variant[28]. Since then, we have been able to apply this methodology to the cytosolic transport of nanobodies as well as the intracellular targeting of fluorescent proteins[29,30]. Still, to achieve transduction of proteins into the cytosol, rather high concentrations of the cargo protein must be applied, ranging from 10 µM of a small antibody fragment (nanobody) to up to over 100 µM of enhanced GFP (EGFP). These concentrations are much higher than those required for the transduction of small cargoes[27] and suggest that there is a size dependence of the cargo on transduction. Consequently, it might not be possible at all to deliver even larger molecules in an energy-independent manner.

Encouraged by previous findings that report the cooperative interaction of arginine-rich CPPs with physiological membranes in a concentration-dependent manner[31–34], we probed the impact of CPPs added to cells in addition to protein–CPP cargoes. Starting with simple cysteine-containing unbound CPPs as additives, we find that thiol reactivity plays an important role in this additive approach, which is consistent with previous reports using

[1]Leibniz-Forschungsinstitut für Molekulare Pharmakologie (FMP), Berlin, Germany. [2]Institute of Chemistry and Biochemistry, Freie Universität Berlin, Berlin, Germany. [3]Technical University of Darmstadt, Darmstadt, Germany. [4]Department of Chemistry, Humboldt-Universität zu Berlin, Berlin, Germany.
✉e-mail: hackenbe@fmp-berlin.de

thiol-reactive cargoes[35,36]. In particular, we show that electrophilic thiol-reactive CPP additives are highly effective at creating nucleation zones on the cell surface, which enable efficient transduction of protein–CPP conjugates. Our protocol proves to be highly effective, simple and not harmful to the cell. Importantly, we show that we can enable the transduction of recombinant CPP-containing proteins as well as a 150-kDa immunoglobulin-G (IgG) antibody into living cells via a non-endosomal uptake mechanism.

Results

Improved cellular uptake of cargoes mediated by cell-penetrating peptide additives. To evaluate the concentration, temperature and cargo size dependency of added arginine-rich peptides in the mediation of cytosolic delivery, we chose three distinct cargoes to transport: the organic fluorophore tetramethylrhodamine (TAMRA, ~450 Da), the camelid-derived anti-GFP nanobody GBP1 (~14 kDa) and the fluorescent protein mCherry with a nuclear localization signal (NLS-mCherry, ~28 kDa). We attached each of the cargoes to a synthetic cyclic R10 (cR10) peptide, yielding an intracellularly non-cleavable conjugate, either via an amide bond in the case of TAMRA or using maleimide chemistry for the proteins (analytical data for the peptides are provided in Supplementary Fig. 1, and characterization of GBP1 and mCherry, and their CPP conjugates, is described in Supplementary Figs. 2 and 3), following our previous reports[29,30]. In all cases, successful cytosolic delivery would lead to staining of the cytosol and of the nucleolus, an RNA-rich membrane-less compartment inside the nucleus (red area in the nucleus, Fig. 1a) for which cationic CPPs have affinity[29,37,38]. The cR10 peptide, consisting of 10 arginines with alternating L and D configurations, has previously been shown to be effective in the delivery of functional proteins, albeit only at relatively high concentrations[29,30]. We then applied all of the synthesized cargoes to HeLa Kyoto cells (expressing nuclear GFP–PCNA[39,40] (PCNA, proliferating cell nuclear antigen) as antigen for the nanobody), at both 37 °C and 4 °C (Fig. 1b–d and individual channels in Supplementary Fig. 4). At 37 °C, the CPP-bearing cargoes can reach the cytosol either via endocytosis and endosomal escape (Fig. 1a) or by directly transducing the membrane, circumventing energy-dependent transport. At 4 °C, however, active transport should not occur, and the cellular fluorescence would be the result of transduction[41,42].

Following incubation of the cells with TAMRA–cR10 for 1 h in cell culture medium, we found cytosolic (and nucleolar) localization of the red fluorophore at only 1 μM, with incubation at both 4 °C and 37 °C (Fig. 1b). These experiments show that successful cytosolic delivery for this small fluorophore can be achieved under conditions without endosomal uptake.

For the nanobody–CPP conjugate, a concentration of 1 μM results in predominantly punctate endosomal fluorescence at 37 °C, whereas at 4 °C the nanobody is excluded from the cell (Fig. 1c). At a concentration of 5 μM, endosomal uptake is less prominent, and uptake also works to some extent at the cold temperature (Supplementary Fig. 4). At 10 μM concentration, all cells show cytosolic (and nucleolar) staining at 37 °C and 4 °C (Fig. 1c). Interestingly, for all proteins we tested, the nucleolar staining is more evident at 37 °C, whereas cytosolic staining is more pronounced at 4 °C, which may be because active nuclear import is also an energy-independent process[43].

Following our proposal, we thought it might be possible to rescue the cytosolic delivery of the protein at low concentrations by adding unbound CPP. Indeed, when we co-incubated 5 μM cysteine-containing cR10 peptide (Cys-cR10, **1**), which we previously used for the semi-synthesis of nanobodies by expressed protein ligation[30], with 1 μM nanobody–cR10 conjugate for 1 h on HeLa cells, the nanobody showed efficient cytosolic and nucleolar staining at both temperatures (Fig. 1c and Supplementary Fig. 4).

For the NLS-mCherry–cR10 conjugate (**I**), the required concentration to achieve cytosolic uptake is even more restrictive, with anything below 50 μM leading to dominant endosomal uptake without nucleolar localization at 37 °C and no uptake at all at 4 °C (Fig. 1d). Analogous to the nanobody experiments, the addition of 5 μM peptide **1** allowed energy-independent transduction of mCherry at a low concentration of 5 μM (Fig. 1d). Delivery could even be achieved at 1 μM protein and 5 μM peptide (Supplementary Fig. 4), although under these conditions the fluorescence of the mCherry was faint and difficult to detect.

Encouraged by these findings, we subsequently probed the performance of linear CPP sequences in the cargo conjugates and additives. Although CPP cyclization is known to improve cell permeability[27,28], we now also observed efficient nucleolar delivery of 5 μM NLS-mCherry linked to a linear R10 peptide (conjugate **II**) with 5 μM of a linear CPP additive (Cys-R10 **2**), in which both sequences consist of 10 L-arginine residues (Fig. 1e). With CPP additive **2**, nucleolar red fluorescence could be detected in more than 90% of cells, but in less than 5% without the additive (Supplementary Fig. 5). As a comparison, we tested the delivery of mCherry–R10 **II** in the presence of 10 or 150 μM endosomolytic peptide ppTG21[44,45]. Neither concentration led to efficient endosomal release, instead leading to the formation of large, fluorescent aggregates in cells (Supplementary Fig. 5).

Finally, we performed uptake at 37 °C with NLS-mCherry–R10 **II** and CPP additive **2** in the presence of Alexa647-labelled transferrin (which undergoes receptor-mediated endocytosis[46,47]) and endocytosis inhibitors (sodium azide, Dynasore and pitstop 2). Although we could see inhibition of the endocytosis of transferrin, we could detect nucleolar mCherry, regardless of the inhibitor used (Supplementary Fig. 6).

A thiol-reactive deca-arginine is a highly effective additive for delivering CPP-conjugated proteins. To further evaluate the high efficiency of the CPP-peptide additives **1** and **2** in our additive protocol and to probe the impact of the N-terminal thiol functionality, we synthesized additional linear CPPs **3**–**5** with different thiol derivatives (Fig. 2a). We then co-delivered 5 μM CPP conjugates of mCherry linked either to a linear (**II**) or cyclic R10 (**I**) (as in Fig. 1d,e) together with the newly synthesized peptides **1**–**5** into HeLa Kyoto cells and used microscopy to measure both nuclear and total fluorescence (representative pictures for all tested conditions are presented in Supplementary Fig. 7). In this way, we quantified the desirable delivery to the nucleus and nucleoli (Fig. 2a), and also the amount of unwanted endosomal entrapment (Supplementary Fig. 8; for details see Supplementary Methods). Using unconjugated mCherry as a cargo did not result in any detectable intracellular fluorescence, while using mCherry–R10 conjugate **II** in combination with additive R10 peptide **2** led to nuclear/nucleolar staining, as before (Fig. 2a, first two bars).

To exclude thiol-based interactions of the peptide, we capped the N-terminal Cys residue with iodoacetamide in CPP **3**. With **3**, we observed a sharp decrease in the efficiency of nuclear protein delivery in comparison to additive **2** (Fig. 2a, grey and mint bars). To probe a potential dimerization of the CPP, following the previous observation of using disulfide-linked TAT dimers[21], we employed the dimer of Cys-R10 (**4**, red bar). However, no increase in efficiency over using monomer **2** was visible in this case.

Based on these observations, we hypothesized that the better delivery using peptide additive **2** is due to the formation of disulfide bridges on the cell surface[48,49]. We thus synthesized a thio-nitro-benzoic-acid-activated R10 peptide (TNB-R10, **5**), which carries an electrophilic disulfide to accelerate disulfide formation. Indeed, we observed more than 50% increase in nuclear mCherry fluorescence intensity compared to that of the Cys-variant **2** (blue bar, Fig. 2a), as well as a significant increase in the fraction of nuclear fluorescence (Supplementary Fig. 8).

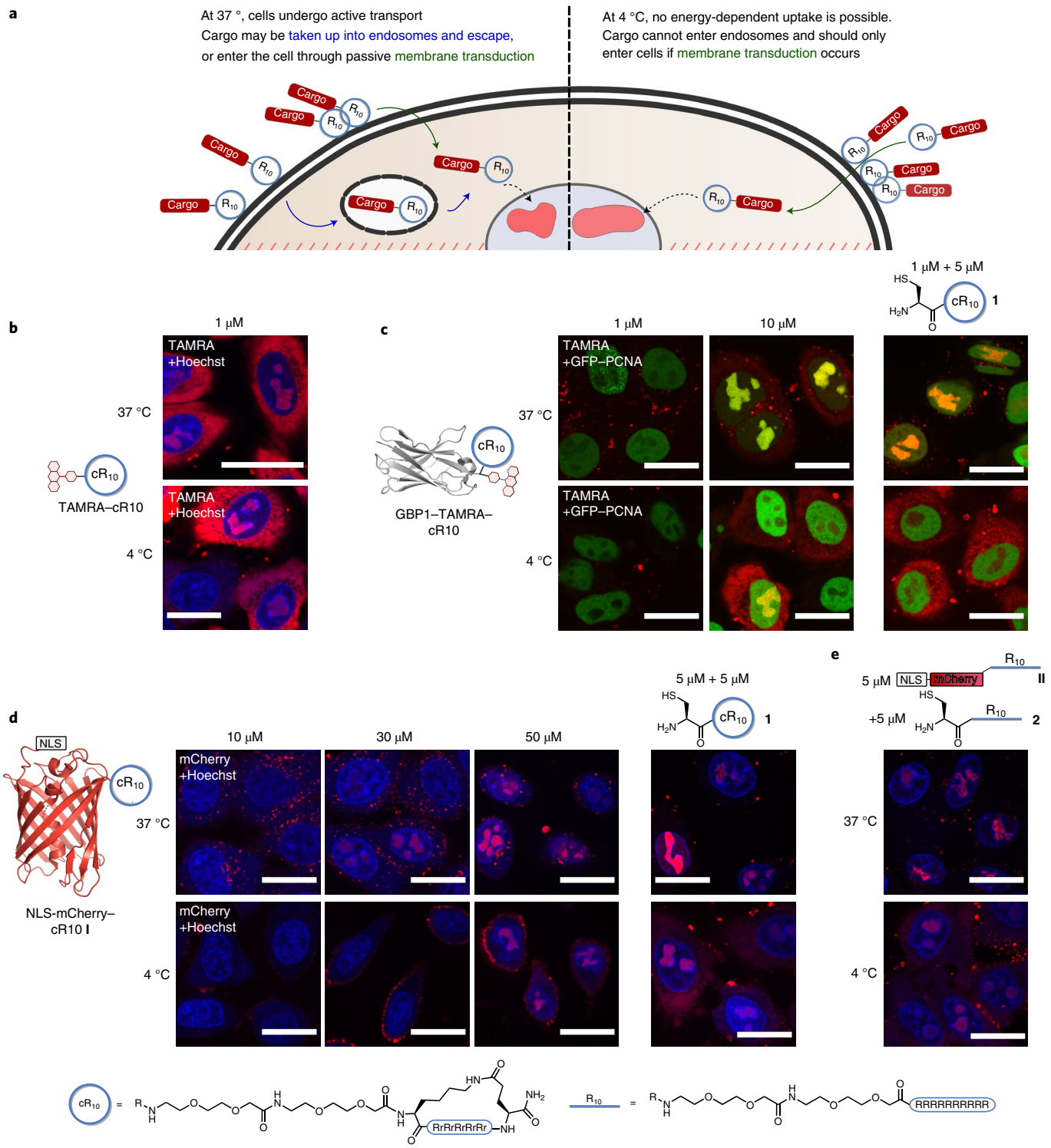

Fig. 1 | Concentration-dependent delivery of CPP-bearing red fluorescent cargoes into HeLa Kyoto cells at 37 °C and 4 °C. a, The different modes of uptake at 37 °C and 4 °C. **b**, Cellular uptake of TAMRA–cR10 at 37 °C and 4 °C and a concentration of 1 μM. **c**, Cellular uptake of fluorescently labelled GBP1 nanobody (PDB structure 3K1K) with cR10 peptide at 37 °C and 4 °C and concentrations of 1 and 10 μM, as well as at 1 μM concentration with 5 μM additional cR10 **1**. Here, nuclear GFP fluorescence of the GFP–PCNA fusion protein is shown instead of the Hoechst staining. **d**, Cellular uptake of cR10-modified NLS-mCherry **I** (PDB 2H5Q) at 37 °C and 4 °C and concentrations of 10, 30 and 50 μM, as well as at 5 μM concentration with 5 μM additional cR10. **e**, Cellular uptake of linear R10-modified NLS-mCherry **II** with added 5 μM linear R10 **2**. Scale bars, 20 μm. Uppercase R is L-arginine and lower case r is D-arginine. Split channel images and additional concentrations are described in Supplementary Fig. 4.

Using the cyclic R10 peptide **1** as co-delivery agent decreased the uptake efficiency (Fig. 2a, brown bar), but using the mCherry conjugate with the cyclic R10 (**I**) made the delivery with additive **2** even more efficient (Fig. 2a, orange bar).

By far the highest nuclear fluorescence was observed with conjugate (**I**) in combination with the electrophilic disulfide additive **5** (Fig. 2a, green bar), although endosomal fluorescence was also increased under these conditions (Supplementary Fig. 8).

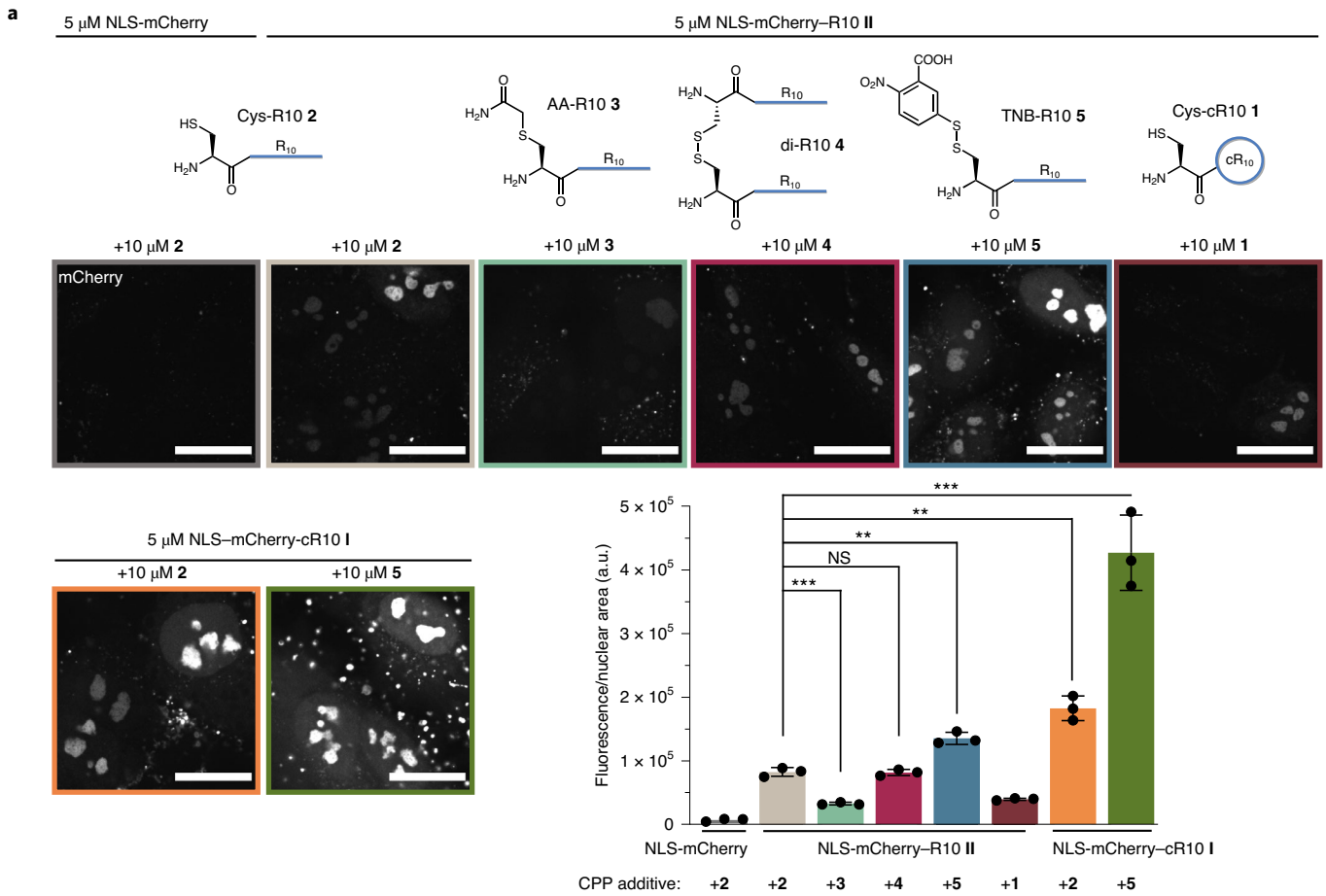

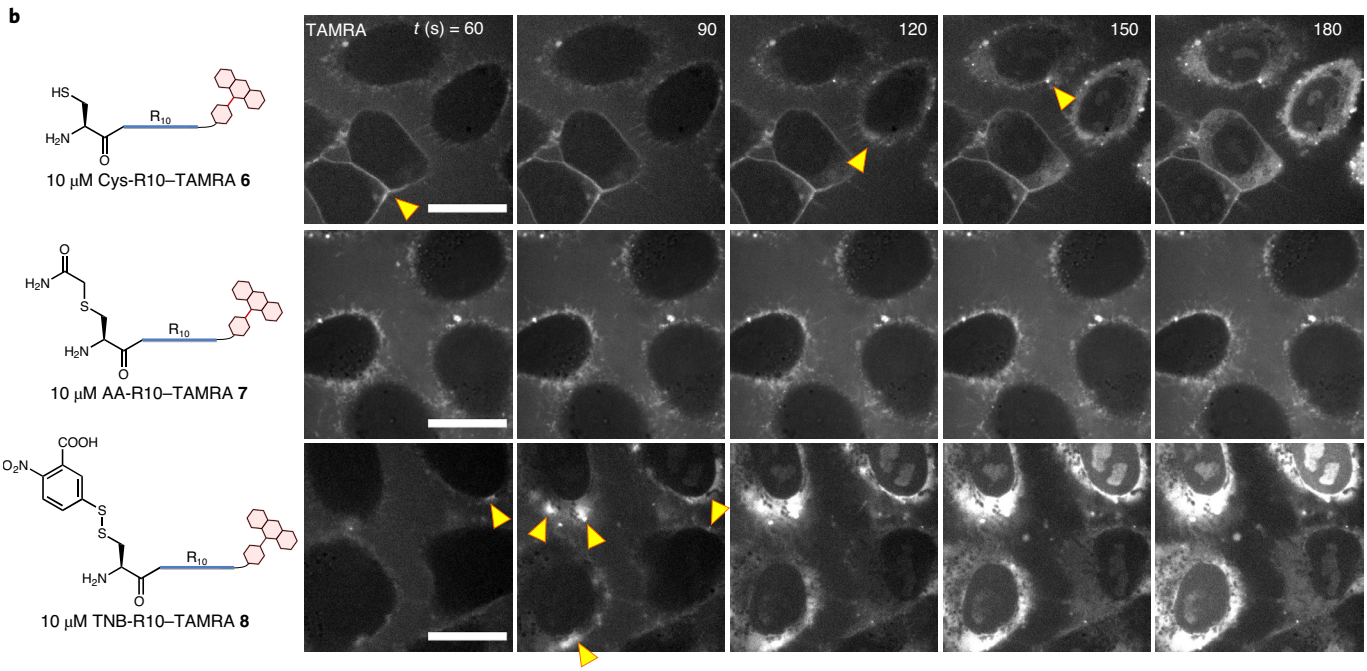

Fig. 2 | TNB-R10 and its performance in delivering CPP-bearing cargoes into cells. a, Quantitative microscopy data showing the mean fluorescence intensity in the nucleus of mCherry–R10 conjugates **I** and **II** with R10 peptides **1**–**5**, as well as representative microscopy images (images of at least 150 cells were taken in triplicate for each condition). Data in the bar chart are presented as individual values and mean ± standard deviation. Two-sided Student's *t*-test; $P = 0.0003$ for mCherry–R10 with Cys-R10 compared to AA (acetamide)-Cys-R10; $P = 0.0015$ for mCherry–R10 with Cys-R10 compared to mCherry–R10 with TNB-R10; $P = 0.0011$ for mCherry–R10 with Cys-R10 compared to mCherry–cR10 with Cys-R10; $P = 0.0006$ for mCherry–R10 with Cys-R10 compared to mCherry–R10 with TNB-R10. ***$P < 0.0005$, **$P < 0.005$; NS, not significant. **b**, Time-lapse experiments showing the cellular uptake of fluorescent R10 peptides with different head groups. Yellow arrowheads indicate nucleation zones where fluorescence is enriched before uptake into the cell. Scale bars, 20 μm.

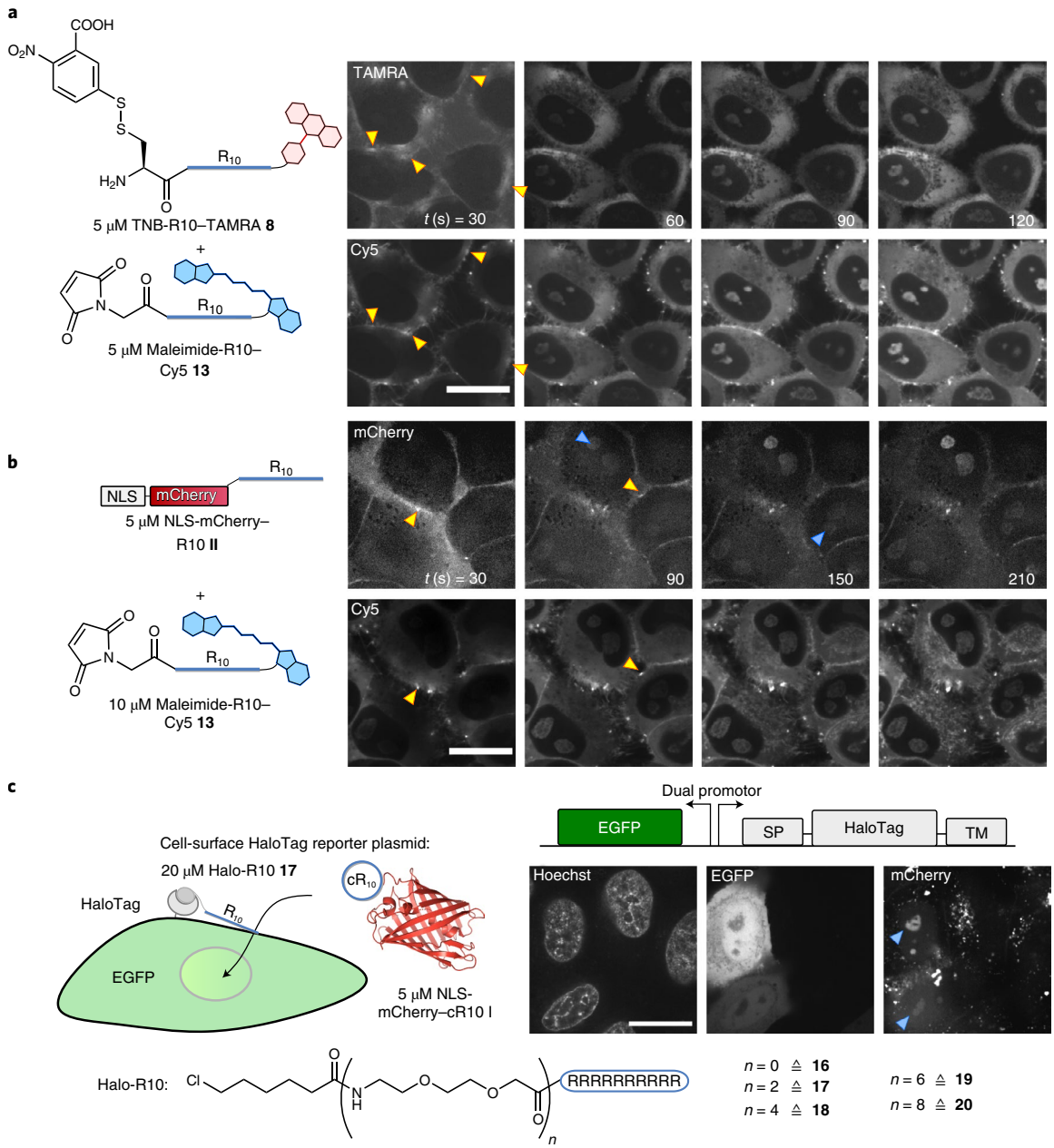

Fig. 3 | Protein transduction into cells through CPP-labelled cell membranes. a, Time-lapse experiment of the simultaneous uptake of the TNB-R10–TAMRA **8** and maleimide-R10–Cy5 **13** peptides into cells in cell medium. Yellow arrowheads indicate nucleation zones stained by both peptides. **b**, Time-lapse of the co-delivery of NLS-mCherry–R10 **II** together with the maleimide-R10–Cy5 peptide **13** on HeLa Kyoto cells in cell medium. Yellow arrowheads indicate nucleation zones and blue arrowheads the appearance of nucleolar staining of the mCherry. **c**, Cellular uptake of NLS-mCherry–cR10 **I** in the presence of chloroalkane-modified 'Halo-R10' **17** on HeLa Kyoto cells transfected with EGFP-transmembrane-HaloTag plasmid (1 h at 37 °C in cell medium). SP, signal peptide; TM, transmembrane sequence. Blue arrowheads indicate mCherry in the nucleoli of EGFP-positive cells. Uptake experiments with peptides **16** and **18**–**20** are described in Supplementary Fig. 21. Scale bars, 20 μm.

Another clear advantage of using an additive to control the cytosolic delivery of cargoes is that it may allow more control over the delivered cargo concentration. To test this proposal, we added various amounts of NLS-mCherry–R10 to cells, together with a constant concentration of peptide additive **5**. We could see a linear relationship between the amount of mCherry added to the cells and the resulting nucleolar fluorescence, indicating that it is possible to precisely titrate a cargo into cells (Supplementary Fig. 9).

To obtain a better understanding of how the cysteine- and TNB-containing peptide additives perform better in cargo delivery, we synthesized fluorescent variants **6**–**8** of peptides **2**, **3** and **5**. We performed time-lapse uptake experiments of the peptides alone at 5, 10 and 20 μM concentration (Fig. 2b; the complete dataset is provided in Supplementary Fig. 10). All peptides showed rapid uptake into cells at 20 μM concentration, immediately after the appearance of bright spots on the membrane, which were previously described as 'nucleation zones'[13,50]. At 10 μM concentration, the acetylated peptide **7** did not show any uptake during the first 3 min, whereas the uptake was already complete for **6** and **8** (Fig. 2b). Notably, the TNB-modified peptide **8** (Fig. 2b, bottom row) showed very quick uptake and very frequent formation of nucleation zones (yellow arrowheads, enlarged insets in Supplementary Fig. 10). Similar

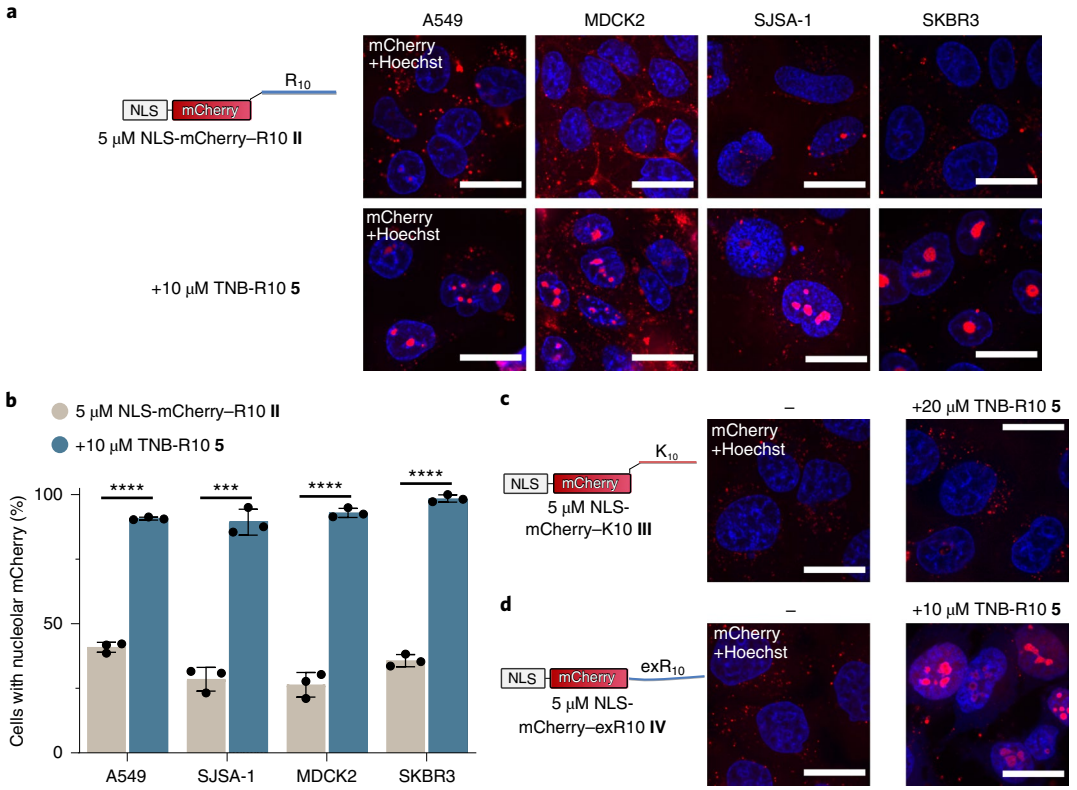

Fig. 4 | Co-delivery with cysteine-reactive R10 peptides in different cell lines and with different cargoes. a, Confocal microscopy images of four cancer cell lines treated with mCherry–R10 **II** and TNB-R10 **5**, for 1 h at 37 °C. **b**, Quantification of cells showing nucleolar fluorescence. At least 150 cells were counted over three biological replicates. Shown are individual values and mean ± standard deviation. Two-sided Student's *t*-test comparing mCherry–R10 **II** (grey) and mCherry–R10 **II** and TNB-R10 **5** (blue); $P < 0.0001$ for A549 cells; $P = 0.0001$ for SJSA-1 cells; $P < 0.0001$ for MDCK2 cells; $P < 0.0001$ for SKBR3 cells. $^{****}P < 0.0001$, $^{***}P < 0.0005$. **c**, Cellular uptake of K10-modified mCherry with or without TNB-R10 **5** at 37 °C leads to endosomal staining and no nucleolar fluorescence. **d**, Cellular uptake of mCherry with recombinant R10 (exR10) shows endosomal or nucleolar staining in the absence and presence of TNB-R10 **5**, respectively.

observations could also be made with 5 μM peptide, although uptake was slower (Supplementary Fig. 10). These findings suggest that the thiol-reactive head groups assist the peptide in forming these zones and crossing the membrane.

To ensure that this effect is due to the thiol reactivity of the TNB group, we pre-treated cells with a thiol-reactive maleimide that should at least partially block the accessible cell-surface thiols. After this pre-treatment, uptake of the TNB-R10 **8** was indeed slowed down considerably (Supplementary Fig. 11). The peptide was also not taken up at all in the presence of the anionic polysaccharide heparin (Supplementary Fig. 11), showing that the electrostatic interactions between the polyarginine and cell are also crucial for uptake. We also investigated the addition of free, reduced cysteine into the cell medium during uptake[51]. Addition of cysteine neither sped up the uptake of the acetylated peptide **7** (Supplementary Fig. 12) nor slowed down the uptake of the cysteine-containing peptide **6** (Supplementary Fig. 13).

To verify that these effects are independent of the position of the cysteine within the peptide, we also synthesized two additional cysteine-containing, fluorescent R10 peptides in which the cysteine was in a different position (within the polyarginine sequence or at the C terminus). These peptides showed comparable rates of uptake to the previous peptide and they were also much faster than their acetylated counterparts (peptides **9**–**12**, Supplementary Fig. 14).

Covalent immobilization of CPPs on the cell surface allows delivery of large cargoes through the membrane. Next, we wanted to explore other cysteine-selective reactions in this context. Maleimides are also thiol-selective and form more stable bonds (under biological conditions) than disulfides, which makes characterization easier. We first wanted to confirm that there are addressable, surface-exposed thiols on cells. To that end, we labelled cells with a cell-impermeable, maleimide-functionalized fluorophore (Supplementary Fig. 15). The fluorophore showed effective membrane staining, which could be strongly reduced by first blocking thiols on the cells with Ellman's reagent (Supplementary Fig. 15).

We then synthesized a fluorescent, maleimide-functionalized linear R10 (maleimide-R10–Cy5) **13**, which can be traced separately by fluorescent microscopy. First, we wanted to confirm that this peptide shows uptake behaviour similar to that of the fluorescent TAMRA-labelled TNB-activated R10 peptide **8**. Indeed, when the two fluorescent peptides are incubated with cells simultaneously, they stain the same nucleation zones and are taken up at similar rates (Fig. 3a and Supplementary Fig. 16), and peptide **13** also shows staining of nucleation zones alone (Supplementary Fig. 16).

We then co-delivered R10-modified mCherry **II** together with the newly synthesized maleimide-R10–Cy5 peptide **13** (Fig. 3b and Supplementary Fig. 16c). We observed that the protein was localized at the same nucleation zones and is subsequently taken up into cells, although the protein requires more time to reach the nucleolus (note the longer steps in the time-lapse experiment). This observation supports the assumption that the protein crosses nucleation zones, which are 'pre-labelled' by the reactive peptide additives.

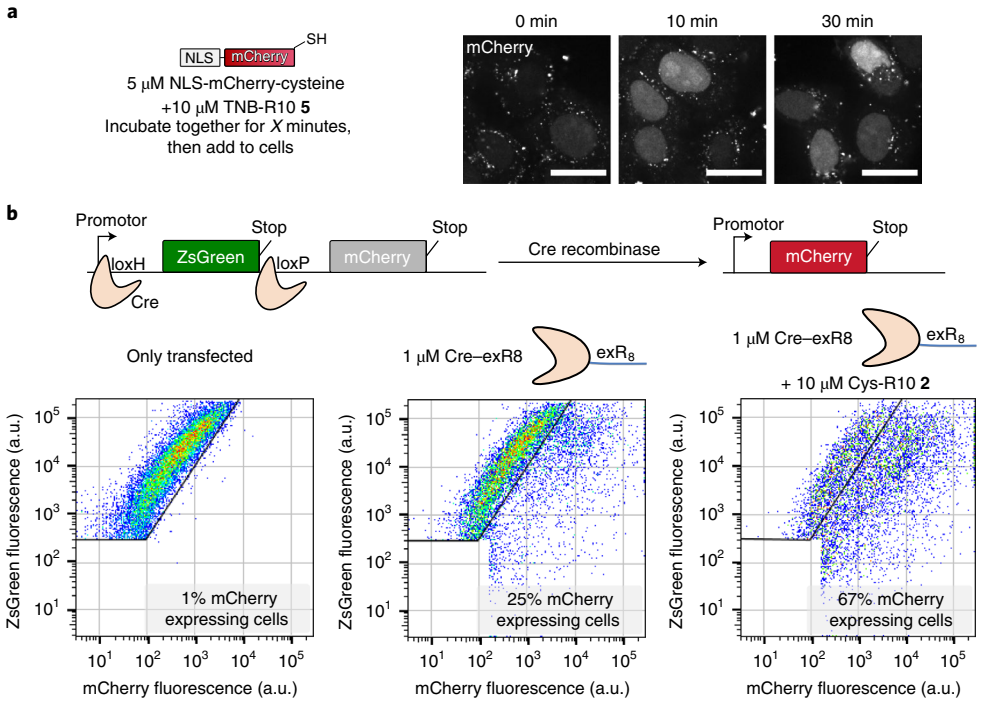

Fig. 5 | Delivery of cysteine-containing mCherry and recombinant R8-containing Cre recombinase. a, Disulfide CPP modification of mCherry and in situ cellular uptake. Scale bars, 20 μm. **b**, Scheme showing the Cre stoplight reporter plasmid and flow cytometry data of HeLa CCL-2 cells transfected with it and subsequently treated with Cre–exR8 with or without Cys-R10 (**2**). ZsGreen, green fluorescence protein.

As additional evidence for the covalent modification of a membrane component with **13**, we treated cells with the peptide and subsequently washed the cells with either medium or 50 μM Triton X-100 to remove unbound peptide. The peptide stained membranes, even after washing with the detergent (Supplementary Fig. 17). We also treated cells with **13** and delivered NLS-mCherry–R10 **II** into these cells after washing with 25 μg ml^{-1} heparin (Supplementary Fig. 18). Washing with heparin should remove cell-penetrating peptides that are non-covalently bound to the cell membrane[20]. The successful delivery of mCherry **II** suggests that the covalently bound peptide can be sufficient for protein delivery.

To explore this concept further, we treated cells with peptides **2**, **3** or **5** or with a non-fluorescent maleimide-R10 peptide **14** in a first step. After certain time points, we removed the peptide solution and added the R10-conjugated mCherry **II** (Supplementary Fig. 19). For the maleimide- and TNB-R10 peptides **5** and **12**, we could still observe nuclear delivery after 5 min of 'pre-labelling' with the peptide, and successful, albeit reduced, delivery of mCherry **II** after 30 min.

To identify potential reaction partners of the cysteine-reactive peptides, we synthesized a biotinylated version of the maleimide-R10 peptide (**15**) and applied it to cells followed by a streptavidin pull-down, tryptic digestion and protein identification by mass spectrometry. Label-free quantification of identified proteins revealed several membrane proteins enriched by the R10 peptide over untreated cells and a biotin-maleimide control (Supplementary Fig. 20). This suggests that there is no single target but rather several proteins with which the peptides can react.

To investigate changes in the membrane at nucleation zones, we performed uptake of CPPs in the presence of the phosphatidylserine-binding protein annexin V. It had previously been suggested that the accumulation of CPPs at nucleation zones leads to a local membrane inversion, facilitating cargo uptake[52]. We could not detect any enrichment of phosphatidylserine (Supplementary Fig. 21); however, we employed Flipper-TR, a fluorescent membrane tension probe[53], and could observe a reduction of membrane tension at nucleation zones, which points to a local deformation of the membrane (Supplementary Fig. 22).

Taken together, our results support that thiol-reactive CPPs increase cellular delivery of cargoes through the covalent linking of peptides to the cell membrane. To elaborate this further, we generated a plasmid that would lead to expression of an EGFP reporter inside transfected cells along with a HaloTag[54] on the cell surface (a simplified plasmid map is shown in Fig. 3c; validation of the plasmid and additional controls are presented in Supplementary Fig. 23). We then synthesized a series of chloroalkane-modified R10 peptides **16**–**20** with varying polyethylene glycol linker lengths for covalent labelling of the expressed HaloTag. We added 'Halo-R10' peptides **16**–**20** to the cells together with NLS-mCherry–cR10 **I**. We observed no nucleolar staining for the peptide with no ethylene glycol between the chloroalkane and the R10 peptide (Supplementary Fig. 23). For all peptides containing a linker, we saw nucleolar mCherry staining in transfected cells (Fig. 3c, blue arrowheads, cells showing EGFP signal; see Supplementary Fig. 23 for peptides **18**–**20**), but not in untransfected cells. However, all cells showed endosomal uptake and 20 μM Halo-R10 was needed to achieve nucleolar staining. This lower efficiency may be due to the limited amount and reactivity of the HaloTag protein on the cell surface.

Cargo delivery using TNB-R10 is robust in various cell lines and accepts recombinant protein cargoes. To test if membrane transduction of proteins can be achieved in different cell lines, we tested our protocol in four additional cancer cell lines with different tissue origin (A549, MDCK2, SJSA-1 and SKBR3). We recorded the uptake and nucleolar staining of 5 μM mCherry–R10 **II** in the presence of 10 μM TNB-R10 **5** in all tested cell lines at 37 °C (Fig. 4a,b and Supplementary Fig. 24) and 4 °C (Supplementary Fig. 25).

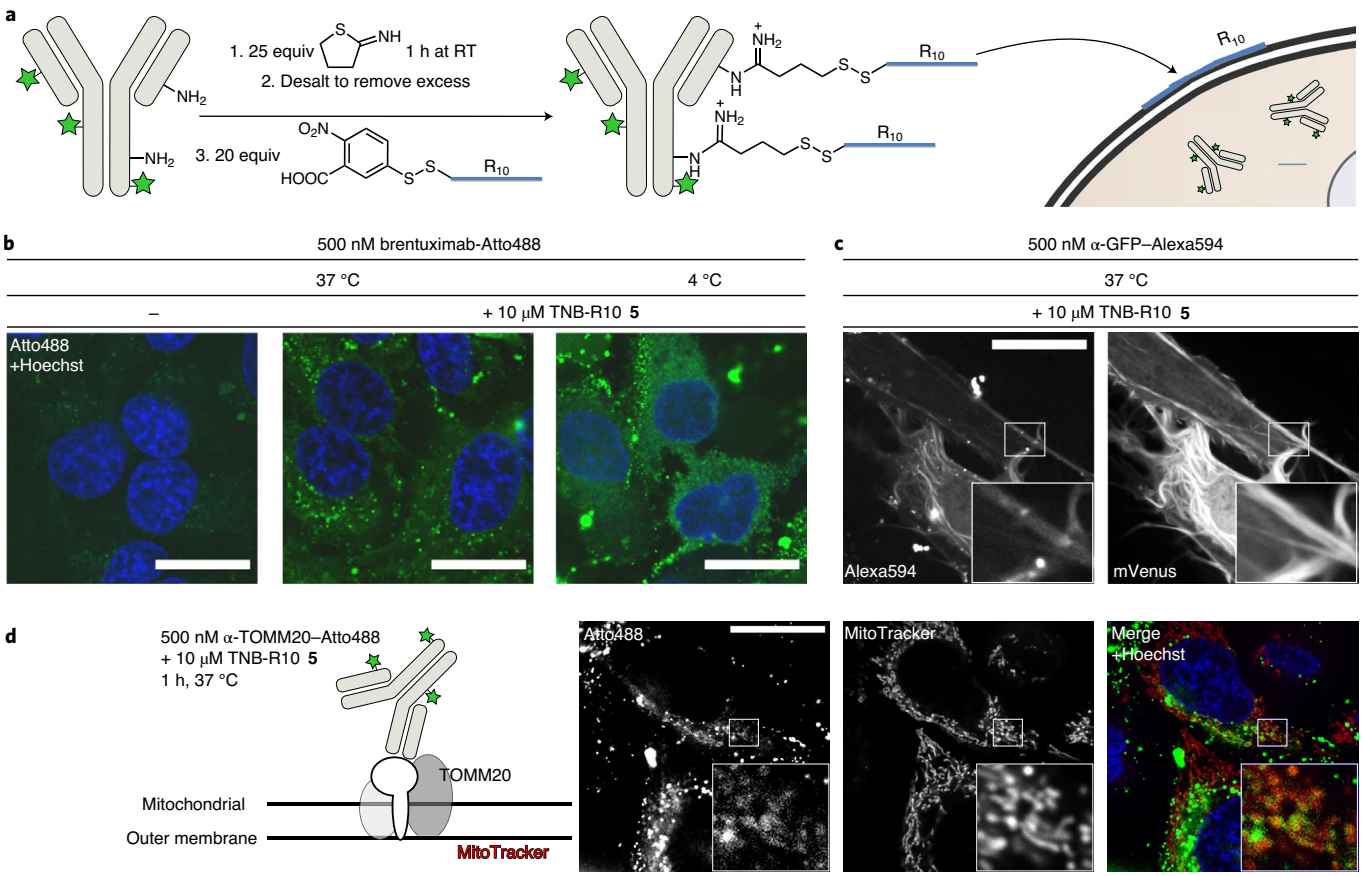

Fig. 6 | The application of TNB-R10 in IgG antibody delivery. a, Method of delivering antibodies into cells using TNB-R10. **b**, Cellular uptake of 500 nM Atto488-labelled brentuximab into HeLa CCL-2 cells in the presence and absence of TNB-R10 **5** and at 37 °C and 4 °C. Cells are counterstained with Hoechst 33342 to demonstrate exclusion of the antibody from the nucleus. **c**, Cellular uptake of 500 nM Alexa 594-labelled anti-GFP antibody into HeLa CCL-2 cells transfected with LifeAct-mVenus. **d**, Cellular uptake of 500 nM Atto488-labelled anti-TOMM20 antibody into HeLa CCL-2 cells, simultaneously treated with MitoTracker Red CMXRos. Scale bars, 20 μm.

Most of our findings point to an energy-independent mode of uptake, but to probe whether TNB-R10 **5** can also lead to endosomal leakage of an entrapped cargo, we used peptide **5** on cells in combination with an mCherry variant (NLS-mCherry–K10 **III**) that had been modified with a K10 peptide (via maleimide chemistry, Supplementary Fig. 3). The K10 peptide should be sufficient to bring the protein into contact with the cell membrane and deliver it into endosomes through active transport, but should not transduce, as lysine-rich peptides do not share the crucial characteristics of arginine-rich peptides for the membrane interaction[33,55]. Indeed, incubation of 5 μM mCherry–K10 alone or in combination with 20 μM peptide **5** did not lead to nuclear localization, but only the punctate fluorescence indicative of endosomal entrapment (Fig. 4c and Supplementary Fig. 26).

Additionally, peptide **5** showed no signs of cytotoxicity or decreased cell viability up to 50 μM peptide (Supplementary Fig. 27). Cells that took up mCherry with or without **5** showed staining with calcein AM (acetoxymethylester), a cell-permeable caged fluorophore that shows intracellular fluorescence in cells with active metabolism (Supplementary Fig. 27). Performing uptake in the presence of the dead cell stain Sytox Blue also did not lead to nuclear staining with the dye (Supplementary Fig. 27). Taken together, these experiments suggest that TNB-R10 peptide **5** does not lead to disruption of the endosomal or cellular membrane.

Methods of cargo delivery that rely on endosomal escape are often susceptible to the presence of serum, as they require effective endocytosis of both the cargo and the endosomolytic agent[21]. We hypothesized that peptide **5** would probably react with thiols in the serum, but the co-delivery with **2** (Cys-R10) should still function. Although the presence of serum did lead to reduced efficiency at 10% serum, with 5% serum or lower there was a negligible effect on uptake (Supplementary Fig. 28). Interestingly, even in the presence of serum, the thiol-containing peptide **2** performed significantly better than the alkylated variant **3** (Supplementary Fig. 28). The reduction in efficiency in the presence of large amounts of serum may be due to the thiols in serum or the unspecific binding of CPPs to serum proteins[27].

We also tested if recombinantly expressed CPP fusion proteins can be delivered, as these require much less equipment and effort to produce. To test this, we expressed and purified mCherry with a C-terminal R10 peptide (NLS-mCherry–exR10 **IV**; characterization is provided in Supplementary Fig. 29). The mCherry–exR10 showed similar behaviour to the semi-synthetic variant, showing predominantly endosomal uptake alone at a low, 5 μM concentration, which can be efficiently rescued by addition of peptide **5** (Fig. 4d and Supplementary Fig. 30). This mCherry variant does not contain any cysteines, meaning it cannot form a disulfide with **5**, thus demonstrating that the recombinant polyarginine is enough for co-transport.

In the same vein, we also made mCherry variants modified with R5 and R8 peptides and co-delivered them into cells with TNB-R10 **5** (Supplementary Figs. 31 and 32). The R8 peptide

showed comparable results to the R10 peptide, while we saw a clear drop in efficiency with the R5 peptide.

Given that peptide **5** can readily react with thiols, we tested if applying a labelling mixture of a protein containing a free thiol and CPP additive **5** without intermediate work-up would facilitate the uptake protocol. On mixing 5 μM mCherry with a free cysteine with 15 μM peptide **5**, the cell permeability of the mCherry was already visible after 10 min, which further improved after a 30-min incubation (Fig. 5a). This same protocol also worked well for a cysteine-containing fluorescent nanobody (Supplementary Fig. 33). It should be noted, here, that the CPP is linked to both protein cargoes via an intracellularly cleavable disulfide, which results in broad nuclear staining (because of a nuclear antigen for the nanobody) rather than the nucleolar localization observed before[29,30].

To challenge our delivery protocol, we expressed and purified Cre recombinase fused to a C-terminal R8 peptide (Cre–exR8; for characterization see Supplementary Fig. 34). Fusions of Cre recombinase with the arginine-rich HIV TAT peptide have been reported previously to aid in cell uptake[56]. We transfected HeLa cells with a Cre activity reporter plasmid (Cre Stoplight 2.4[57]) that leads to a change in fluorescence from green to red when the enzyme is present within cells (Fig. 5b). We then treated cells with 1 μM Cre–exR8 alone or with added 10 μM Cys-R10 **2** in the presence of 5% serum, then monitored expression of the reporter gene by flow cytometry and microscopy. As expected, the addition of peptide led to a strong increase in expression of the Cre reporter, indicating successful delivery of active Cre into the nucleus (Fig. 4f; for microscopy results see Supplementary Fig. 35).

The TNB-R10 CPP additive allows cytosolic delivery of functional IgG antibodies. Antibodies are exceptionally useful proteins in molecular biology and pharmacology, targeting most of the human proteome. Nevertheless, the cellular delivery of full-length antibodies is particularly challenging due to the complex and quite large architecture with a molecular weight of 150 kDa and length of 15 nm (approximately). Some methods to deliver full-length antibodies into cells already exist, although they mostly rely on endosomal escape[21,23]. To test whether we can deliver a full-length IgG antibody into cells at 4 °C, we first used the fluorescently labelled therapeutic antibody brentuximab. Thiolation was performed with 2-iminothiolane[58]. As before, by adding peptide **5**, the antibody can be modified with the cell-penetrating peptide via a disulfide bond, while the excess cell-penetrating peptide should simultaneously aid in cellular uptake (Fig. 6a). Indeed, treatment of cells with the antibody led to cellular delivery at 37 °C, but not in the absence of CPP additive **5** (Fig. 6b). A fluorescent signal could not be observed in the nucleus (counterstained with Hoechst), probably because of the size of the antibody excluding it from permeating through nuclear pores. Even at 4 °C, antibody uptake could also be observed in most cells, demonstrating energy-independent membrane transduction of an antibody (Fig. 6b).

To validate that the delivered antibodies are still intact and functional after cellular uptake, we subsequently tested two additional commercial antibodies in our protocols. We first transfected a plasmid encoding a GFP mutant (LifeAct-mVenus) into HeLa cells and functionalized a fluorescently labelled (Alexa 594) anti-GFP antibody as before. Incubation of cells with the antibody showed uptake of the antibody into cells and co-localization of the antibody and mVenus signals within the cell (Fig. 6c, Pearson correlation coefficient (PCC) for the shown inset, 0.80).

Finally, we also tested an antibody against the endogenous mitochondrial receptor TOMM20. As with brentuximab, we first fluorescently labelled the antibody, followed by thiolation and mixing with CPP additive **5**. Incubation of HeLa cells with the mixture and a mitochondrial marker (MitoTracker Red CMXRos) led to noticeable endosomal entrapment, but also visible co-localization of the two components (Fig. 6d, PCC for the shown inset, 0.58).

Discussion

Over recent years, a diverse array of methods for the delivery of biomolecules into cells have been developed[2], but we believe that cell-penetrating, peptide-mediated delivery is among the top methodologies, particularly in terms of synthetic flexibility. Nevertheless, advancing the delivery of CPP–protein and CPP–antibody conjugates with even better uptake properties remains challenging and requires often laborious chemical protein engineering.

Through our work, we have shown the delivery of various cargoes with both synthetic and recombinant CPPs using thiol-reactive R10 peptides. This uptake seems to be independent of active transport and is not harmful to the cell. Cysteine and thiol-reactive species have been described in the context of cellular uptake before[35,36]. The thiol reactivity of the CPPs we describe seems to be a crucial factor in our additive protocol and, in investigating it further, we find that we can covalently label cell surfaces, through which we can then deliver cargoes. We believe that this may develop into a valuable tool for achieving cell-specific delivery of cargoes, if one can only modify cells of a certain type. This could have great therapeutic potential, for example in gene editing, and should be pursued further.

As the TNB-R10 **5** also reacts quickly with thiol residues on biomolecules to form bioreversible disulfide bonds, it allows a 'covalent transfection' that is immediately applicable to many protein substrates. Importantly, no purification is required after addition of the peptide, because the excess directly acts as the CPP additive, thereby strongly enhancing uptake of the protein cargo. Furthermore, we show that even IgG antibodies without any free cysteines can be thiolated to allow use of peptide **5**, and the thiolation could, in principle, also be done in a reversible manner.

An essential benefit of our protocol is the possibility to perform uptake at 4 °C. Under these conditions, no active endosomal uptake occurs, which allows the delivery of compounds that are sensitive to endosomal degradation or are toxic for the cell upon prolonged exposure. Another key advantage of our findings is the ability to employ proteins from standard recombinant expression, in which the protein cargo is genetically fused to an oligo-Arg tag, and use them in non-endocytic uptake. Using these, our protocol allows a straightforward evaluation of CPP additives to enhance uptake. Using this co-delivery strategy, we could deliver active Cre recombinase into cells without any necessary conjugation chemistry. We achieve efficient gene editing, which could easily be applied to the delivery of other functional enzymes. We have demonstrated cytosolic delivery of three different antibodies using CPP additives, resulting in the expected intracellular localization. Because of their high efficiency and lack of measurable cellular toxicity, we envision that our CPP additives will become important tools in cell biology.

This work is an important step in advancing the field of biomolecule delivery, with applications ranging from the intracellular immunostaining demonstrated here to the design of next-generation biopharmaceuticals. Our future work will be directed at making use of this technique in going beyond cell culture to tissue culture and even simple model organisms.

Online content

Any methods, additional references, Nature Research reporting summaries, source data, extended data, supplementary information, acknowledgements, peer review information; details of author contributions and competing interests; and statements of data and code availability are available at https://doi.org/10.1038/s41557-021-00661-x.

Received: 17 December 2019; Accepted: 10 February 2021;
Published online: 15 April 2021

References

1. Fu, A., Tang, R., Hardie, J., Farkas, M. E. & Rotello, V. M. Promises and pitfalls of intracellular delivery of proteins. *Bioconjug. Chem.* **25**, 1602–1608 (2014).
2. Du, S., Liew, S. S., Li, L. & Yao, S. Q. Bypassing endocytosis: direct cytosolic delivery of proteins. *J. Am. Chem. Soc.* **140**, 15986–15996 (2018).
3. Wang, F. et al. Recent progress of cell-penetrating peptides as new carriers for intracellular cargo delivery. *J. Control. Release* **174**, 126–136 (2014).
4. Viscidi, R. P., Mayur, K., Lederman, H. M. & Frankel, A. D. Inhibition of antigen-induced lymphocyte proliferation by Tat protein from HIV-1. *Science* **246**, 1606–1608 (1989).
5. Joliot, A. H., Triller, A., Volovitch, M., Pernelle, C. & Prochiantz, A. α-2,8-Polysialic acid is the neuronal surface receptor of antennapedia homeobox peptide. *New Biol.* **3**, 1121–1134 (1991).
6. Derossi, D., Joliot, A. H., Chassaing, G. & Prochiantz, A. The third helix of the Antennapedia homeodomain translocates through biological membranes. *J. Biol. Chem.* **269**, 10444–10450 (1994).
7. Borrelli, A., Tornesello, A. L., Tornesello, M. L. & Buonaguro, F. M. Cell penetrating peptides as molecular carriers for anti-cancer agents. *Molecules* **23**, 295 (2018).
8. Guidotti, G., Brambilla, L. & Rossi, D. Cell-penetrating peptides: from basic research to clinics. *Trends Pharmacol. Sci.* **38**, 406–424 (2017).
9. Richard, J. P. et al. Cellular uptake of unconjugated TAT peptide involves clathrin-dependent endocytosis and heparan sulfate receptors. *J. Biol. Chem.* **280**, 15300–15306 (2005).
10. Fittipaldi, A. et al. Cell membrane lipid rafts mediate caveolar endocytosis of HIV-1 Tat fusion proteins. *J. Biol. Chem.* **278**, 34141–34149 (2003).
11. Ben-Dov, N. & Korenstein, R. The uptake of HIV Tat peptide proceeds via two pathways which differ from macropinocytosis. *Biochim. Biophys. Acta* **1848**, 869–877 (2015).
12. Herce, H. D., Garcia, A. E. & Cardoso, M. C. Fundamental molecular mechanism for the cellular uptake of guanidinium-rich molecules. *J. Am. Chem. Soc.* **136**, 17459–17467 (2014).
13. Duchardt, F., Fotin-Mleczek, M., Schwarz, H., Fischer, R. & Brock, R. A comprehensive model for the cellular uptake of cationic cell-penetrating peptides. *Traffic* **8**, 848–866 (2007).
14. Futaki, S. & Nakase, I. Cell-surface interactions on arginine-rich cell-penetrating peptides allow for multiplex modes of internalization. *Acc. Chem. Res.* **50**, 2449–2456 (2017).
15. He, L., Sayers, E. J., Watson, P. & Jones, A. T. Contrasting roles for actin in the cellular uptake of cell penetrating peptide conjugates. *Sci. Rep.* **8**, 7318 (2018).
16. Patel, S. G. et al. Cell-penetrating peptide sequence and modification dependent uptake and subcellular distribution of green florescent protein in different cell lines. *Sci. Rep.* **9**, 6298 (2019).
17. Tunnemann, G. et al. Cargo-dependent mode of uptake and bioavailability of TAT-containing proteins and peptides in living cells. *FASEB J.* **20**, 1775–1784 (2006).
18. Verdurmen, W. P., Thanos, M., Ruttekolk, I. R., Gulbins, E. & Brock, R. Cationic cell-penetrating peptides induce ceramide formation via acid sphingomyelinase: implications for uptake. *J. Control. Release* **147**, 171–179 (2010).
19. Takeuchi, T. et al. Direct and rapid cytosolic delivery using cell-penetrating peptides mediated by pyrenebutyrate. *ACS Chem. Biol.* **1**, 299–303 (2006).
20. Wadia, J. S., Stan, R. V. & Dowdy, S. F. Transducible TAT-HA fusogenic peptide enhances escape of TAT-fusion proteins after lipid raft macropinocytosis. *Nat. Med.* **10**, 310–315 (2004).
21. Erazo-Oliveras, A. et al. Protein delivery into live cells by incubation with an endosomolytic agent. *Nat. Methods* **11**, 861–867 (2014).
22. Allen, J. et al. Cytosolic delivery of macromolecules in live human cells using the combined endosomal escape activities of a small molecule and cell penetrating peptides. *ACS Chem. Biol.* **14**, 2641–2651 (2019).
23. Akishiba, M. et al. Cytosolic antibody delivery by lipid-sensitive endosomolytic peptide. *Nat. Chem* **9**, 751–761 (2017).
24. Morris, M. C., Depollier, J., Mery, J., Heitz, F. & Divita, G. A peptide carrier for the delivery of biologically active proteins into mammalian cells. *Nat. Biotechnol.* **19**, 1173–1176 (2001).
25. Reichart, F., Horn, M. & Neundorf, I. Cyclization of a cell-penetrating peptide via click-chemistry increases proteolytic resistance and improves drug delivery. *J. Pept. Sci.* **22**, 421–426 (2016).
26. Dougherty, P. G., Sahni, A. & Pei, D. Understanding cell penetration of cyclic peptides. *Chem. Rev.* **119**, 10241–10287 (2019).
27. Lattig-Tunnemann, G. et al. Backbone rigidity and static presentation of guanidinium groups increases cellular uptake of arginine-rich cell-penetrating peptides. *Nat. Commun.* **2**, 453 (2011).
28. Nischan, N. et al. Covalent attachment of cyclic TAT peptides to GFP results in protein delivery into live cells with immediate bioavailability. *Angew. Chem. Int. Ed.* **54**, 1950–1953 (2015).
29. Schneider, A. F. L., Wallabregue, A. L. D., Franz, L. & Hackenberger, C. P. R. Targeted subcellular protein delivery using cleavable cyclic cell-penetrating peptides. *Bioconjug. Chem.* **30**, 400–404 (2019).
30. Herce, H. D. et al. Cell-permeable nanobodies for targeted immunolabelling and antigen manipulation in living cells. *Nat. Chem.* **9**, 762–771 (2017).
31. Medina, S. H. et al. An intrinsically disordered peptide facilitates non-endosomal cell entry. *Angew. Chem. Int. Ed.* **55**, 3369–3372 (2016).
32. Jones, A. T. & Sayers, E. J. Cell entry of cell penetrating peptides: tales of tails wagging dogs. *J. Control. Release* **161**, 582–591 (2012).
33. Robison, A. D. et al. Polyarginine interacts more strongly and cooperatively than polylysine with phospholipid bilayers. *J. Phys. Chem. B* **120**, 9287–9296 (2016).
34. Shi, J. & Schneider, J. P. De novo design of selective membrane-active peptides by enzymatic control of their conformational bias on the cell surface. *Angew. Chem. Int. Ed.* **58**, 13706–13710 (2019).
35. Aubry, S. et al. Cell-surface thiols affect cell entry of disulfide-conjugated peptides. *FASEB J.* **23**, 2956–2967 (2009).
36. Gasparini, G., Sargsyan, G., Bang, E. K., Sakai, N. & Matile, S. Ring tension applied to thiol-mediated cellular uptake. *Angew. Chem. Int. Ed.* **54**, 7328–7331 (2015).
37. Martin, R. M., Herce, H. D., Ludwig, A. K. & Cardoso, M. C. Visualization of the nucleolus in living cells with cell-penetrating fluorescent peptides. *Methods Mol. Biol.* **1455**, 71–82 (2016).
38. Martin, R. M., Tunnemann, G., Leonhardt, H. & Cardoso, M. C. Nucleolar marker for living cells. *Histochem. Cell Biol.* **127**, 243–251 (2007).
39. Leonhardt, H. et al. Dynamics of DNA replication factories in living cells. *J. Cell Biol.* **149**, 271–280 (2000).
40. Chagin, V. O. et al. 4D Visualization of replication foci in mammalian cells corresponding to individual replicons. *Nat. Commun.* **7**, 11231 (2016).
41. Hunt, L. et al. Low-temperature pausing of cultivated mammalian cells. *Biotechnol. Bioeng.* **89**, 157–163 (2005).
42. Goldenthal, K. L., Pastan, I. & Willingham, M. C. Initial steps in receptor-mediated endocytosis. The influence of temperature on the shape and distribution of plasma membrane clathrin-coated pits in cultured mammalian cells. *Exp. Cell. Res.* **152**, 558–564 (1984).
43. Melchior, F., Guan, T., Yokoyama, N., Nishimoto, T. & Gerace, L. GTP hydrolysis by Ran occurs at the nuclear pore complex in an early step of protein import. *J. Cell Biol.* **131**, 571–581 (1995).
44. Rittner, K. et al. New basic membrane-destabilizing peptides for plasmid-based gene delivery in vitro and in vivo. *Mol. Ther.* **5**, 104–114 (2002).
45. Rouet, R. et al. Receptor-mediated delivery of CRISPR-Cas9 endonuclease for cell-type-specific gene editing. *J. Am. Chem. Soc.* **140**, 6596–6603 (2018).
46. Mayle, K. M., Le, A. M. & Kamei, D. T. The intracellular trafficking pathway of transferrin. *Biochim. Biophys. Acta* **1820**, 264–281 (2012).
47. Ter-Avetisyan, G. et al. Cell entry of arginine-rich peptides is independent of endocytosis. *J. Biol. Chem.* **284**, 3370–3378 (2009).
48. Gasparini, G. et al. Cellular uptake of substrate-initiated cell-penetrating poly(disulfide)s. *J. Am. Chem. Soc.* **136**, 6069–6074 (2014).
49. Fu, J., Yu, C., Li, L. & Yao, S. Q. Intracellular delivery of functional proteins and native drugs by cell-penetrating poly(disulfide)s. *J. Am. Chem. Soc.* **137**, 12153–12160 (2015).
50. Wallbrecher, R. et al. Membrane permeation of arginine-rich cell-penetrating peptides independent of transmembrane potential as a function of lipid composition and membrane fluidity. *J. Control. Release* **256**, 68–78 (2017).
51. Wei, Y., Tang, T. & Pang, H. B. Cellular internalization of bystander nanomaterial induced by TAT-nanoparticles and regulated by extracellular cysteine. *Nat. Commun.* **10**, 3646 (2019).
52. Hirose, H. et al. Transient focal membrane deformation induced by arginine-rich peptides leads to their direct penetration into cells. *Mol. Ther.* **20**, 984–993 (2012).
53. Colom, A. et al. A fluorescent membrane tension probe. *Nat. Chem.* **10**, 1118–1125 (2018).
54. England, C. G., Luo, H. & Cai, W. HaloTag technology: a versatile platform for biomedical applications. *Bioconjug. Chem.* **26**, 975–986 (2015).
55. Tesei, G. et al. Self-association of a highly charged arginine-rich cell-penetrating peptide. *Proc. Natl Acad. Sci. USA* **114**, 11428–11433 (2017).
56. Peitz, M., Pfannkuche, K., Rajewsky, K. & Edenhofer, F. Ability of the hydrophobic FGF and basic TAT peptides to promote cellular uptake of recombinant Cre recombinase: a tool for efficient genetic engineering of mammalian genomes. *Proc. Natl Acad. Sci. USA* **99**, 4489–4494 (2002).
57. Yang, Y. S. & Hughes, T. E. Cre stoplight: a red/green fluorescent reporter of Cre recombinase expression in living cells. *Biotechniques* **31**, 1040–1031 (2001).
58. Jue, R., Lambert, J. M., Pierce, L. R. & Traut, R. R. Addition of sulfhydryl groups to *Escherichia coli* ribosomes by protein modification with 2-iminothiolane (methyl 4-mercaptobutyrimidate). *Biochemistry* **17**, 5399–5406 (1978).

Reporting Summary. Further information on research design is available in the Nature Research Reporting Summary linked to this Article.

Data availability

The UniProt Homo Sapiens database used is available at https://www.uniprot.org/proteomes/UP000005640. All other relevant data are included in the article and its Supplementary Information. The plasmids generated for this study are available from the authors upon request.

Acknowledgements

We thank members of the Hackenberger laboratory for comments and discussion and K. Kemnitz-Hassanin and I. Kretzschmar for technical support. We thank D. Schumacher and H. Leonhardt for providing the brentuximab antibody. This work was supported by grants from the Deutsche Forschungsgemeinschaft (SPP 1623, SFB 1449 and RTG 2473) to C.P.R.H. (HA 4468/9-1, 9-2) and M.C.C. (CA 198/8-1, 8-2), the GIF, the German–Israeli Foundation for Scientific Research and Development, the Einstein Foundation Berlin (Leibniz-Humboldt Professorship), the Boehringer-Ingelheim Foundation (Plus 3 award) to C.P.R.H. and the Fonds der Chemischen Industrie (FCI) to C.P.R.H. and A.F.L.S. (Chemiefonds fellowship).

Author contributions

A.F.L.S., M.L., M.C.C. and C.P.R.H. conceived the experiments and wrote the manuscript. A.F.L.S. cloned, expressed, purified and characterized proteins, synthesized and characterized peptides and protein–peptide conjugates, and performed uptake, cell viability, microscopy and flow cytometry experiments. M.L. performed microscopy experiments and wrote the quantification script together with A.F.L.S. M.K. performed the calcein AM staining.

Competing interests

The technology described in this Article for the delivery of cargoes into cells using cell-surface-reactive peptides is part of a patent application (EP 21159630.9) by A.F.L.S., M.L. and C.P.R.H.

Additional information

Supplementary information The online version contains supplementary material available at https://doi.org/10.1038/s41557-021-00661-x.

Correspondence and requests for materials should be addressed to C.P.R.H.

Peer review information *Nature Chemistry* thanks Roland Brock, Shiroh Futaki and the other, anonymous, reviewer(s) for their contribution to the peer review of this work.

Reprints and permissions information is available at www.nature.com/reprints.

nature research

Corresponding author(s): Christian P. R. Hackenberger

Last updated by author(s): Jan 6, 2021

Reporting Summary

Nature Research wishes to improve the reproducibility of the work that we publish. This form provides structure for consistency and transparency in reporting. For further information on Nature Research policies, see our Editorial Policies and the Editorial Policy Checklist.

Statistics

For all statistical analyses, confirm that the following items are present in the figure legend, table legend, main text, or Methods section.

n/a	Confirmed	
☐	☒	The exact sample size (*n*) for each experimental group/condition, given as a discrete number and unit of measurement
☐	☒	A statement on whether measurements were taken from distinct samples or whether the same sample was measured repeatedly
☐	☒	The statistical test(s) used AND whether they are one- or two-sided *Only common tests should be described solely by name; describe more complex techniques in the Methods section.*
☒	☐	A description of all covariates tested
☒	☐	A description of any assumptions or corrections, such as tests of normality and adjustment for multiple comparisons
☐	☒	A full description of the statistical parameters including central tendency (e.g. means) or other basic estimates (e.g. regression coefficient) AND variation (e.g. standard deviation) or associated estimates of uncertainty (e.g. confidence intervals)
☐	☒	For null hypothesis testing, the test statistic (e.g. *F*, *t*, *r*) with confidence intervals, effect sizes, degrees of freedom and *P* value noted *Give P values as exact values whenever suitable.*
☒	☐	For Bayesian analysis, information on the choice of priors and Markov chain Monte Carlo settings
☒	☐	For hierarchical and complex designs, identification of the appropriate level for tests and full reporting of outcomes
☐	☒	Estimates of effect sizes (e.g. Cohen's *d*, Pearson's *r*), indicating how they were calculated

Our web collection on statistics for biologists contains articles on many of the points above.

Software and code

Policy information about availability of computer code

Data collection	Gel images: Image Lab version 5.1 (Bio-Rad) Flow Cytometry: LSR Fortessa cell analyzer (BD Biosciences) Microscopy: NIS Elements (Nikon) Aquisition of UV-traces: Empower 3 (Waters) Aquisition of high-resolution mass spectra: MassLynx V4.1 (Waters)
Data analysis	Graphpad Prism 8 was used for statistical analysis. ImageJ version 1.52p and its extension FIJI were used in the automated quantification of microscopy images and in the quantification of pearson's correlation coefficient (using the Coloc2 plugin for FIJI). The MaxEnt 1 tool (Waters) was used to process high-resolution mass spectra. MaxQuant v1.6 was used to identify proteins from the Uniprot Homo Sapiens database. Perseus was used to process the data and generate volcano plots. FlowJo (10.6, FlowJo LLC) was used to process flow cytometry data.

For manuscripts utilizing custom algorithms or software that are central to the research but not yet described in published literature, software must be made available to editors and reviewers. We strongly encourage code deposition in a community repository (e.g. GitHub). See the Nature Research guidelines for submitting code & software for further information.

Data

Policy information about availability of data

All manuscripts must include a data availability statement. This statement should provide the following information, where applicable:

- Accession codes, unique identifiers, or web links for publicly available datasets
- A list of figures that have associated raw data
- A description of any restrictions on data availability

The Uniprot Homo Sapiens database used is available under "https://www.uniprot.org/proteomes/UP000005640". All other relevant data are included in the manuscript, supplementary information or source data files. The plasmids generated for this study are available from the authors upon request.

Field-specific reporting

Please select the one below that is the best fit for your research. If you are not sure, read the appropriate sections before making your selection.

☒ Life sciences ☐ Behavioural & social sciences ☐ Ecological, evolutionary & environmental sciences

For a reference copy of the document with all sections, see nature.com/documents/nr-reporting-summary-flat.pdf

Life sciences study design

All studies must disclose on these points even when the disclosure is negative.

Sample size	No statistical methods were used to predetermine sample size. Where statistical analyses were performed, the sample sizes are listed in the corresponding figure legends. In the quantitative microscopy experiments, variations between biological replicates were small and three replicates were estimated to be sufficient.
Data exclusions	No data was excluded.
Replication	All experiments were repeated at least once with similar results. Where statistical analyses were performed, experiments were performed in at least three biological replicates. The uptake of NLS-mCherry-R10 II with and without additional cell-penetrating peptide (as in Figure 1e) was additionally performed in two different laboratories and cell cultures, giving the same results.
Randomization	Randomization was not applicable to this study as no clinical or animal experiments were done.
Blinding	Blinding was not relevant to this study. In a given experiment all samples were treated equally. For the quantitative microscopy experiments, data was automatically processed using a quantification script.

Reporting for specific materials, systems and methods

We require information from authors about some types of materials, experimental systems and methods used in many studies. Here, indicate whether each material, system or method listed is relevant to your study. If you are not sure if a list item applies to your research, read the appropriate section before selecting a response.

Materials & experimental systems

n/a	Involved in the study
☐	☒ Antibodies
☐	☒ Eukaryotic cell lines
☒	☐ Palaeontology and archaeology
☒	☐ Animals and other organisms
☒	☐ Human research participants
☒	☐ Clinical data
☒	☐ Dual use research of concern

Methods

n/a	Involved in the study
☒	☐ ChIP-seq
☐	☒ Flow cytometry
☒	☐ MRI-based neuroimaging

Antibodies

Antibodies used	Brentuximab was provided by the laboratory of Prof. Heinrich Leonhardt (Ludwig-Maximilians-Universität (LMU) München, Germany) The Alexa Fluor 594 anti-GFP Antibody, Clone 1GFP63 was purchased from BioLegend (USA) The Anti-Tom20/Tomm20, clone 2F8.1 antibody was purchased from Merck kGAA.
Validation	The anti-GFP and anti-Tom20/Tomm20 antibodies are validated for use in immunofluorescence by the manufacturers: https://www.biolegend.com/en-us/products/alexa-fluor-594-anti-gfp-antibody-15599 https://www.merckmillipore.com/DE/de/product/Anti-Tom20-Tomm20-Antibody-clone-2F8.1,MM_NF-MABT166#documentation

The obtained Brentuximab antibody was not used in any application that would require antigen binding and therefore does not need to be validated, but binding was shown in several articles e.g. DOI: 10.1002/anie.201904193

Eukaryotic cell lines

Policy information about cell lines

Cell line source(s)	HeLa CCL-2: ATCC HeLa Kyoto (CVCL_1922): Narumiya S.; Kyoto University; Kyoto; Japan. HeLa Kyoto GFP-PCNA: Tu Darmstadt, J Cell Biol 149, 271-280. SK-BR-3: ATCC A549: ATCC MDCK-2: ATCC SJSA-1: ATCC
Authentication	The cell lines were not authenticated.
Mycoplasma contamination	The cell lines were not tested for mycoplasma contamination.
Commonly misidentified lines (See ICLAC register)	No commonly misidentified cell lines were used.

Flow Cytometry

Plots

Confirm that:

☒ The axis labels state the marker and fluorochrome used (e.g. CD4-FITC).

☒ The axis scales are clearly visible. Include numbers along axes only for bottom left plot of group (a 'group' is an analysis of identical markers).

☒ All plots are contour plots with outliers or pseudocolor plots.

☒ A numerical value for number of cells or percentage (with statistics) is provided.

Methodology

Sample preparation	HeLa Kyoto cells were seeded onto a 12-well plate on day 1 of the experiment. On day 2, the Cre-Stoplight 2.4 reporter plasmid was transfected using lipofectamine 2000 according to the manufacturer's protocol. On day 3, the cells were treated with Cre recombinase in medium with 5% serum (or only medium for the control). The cells were incubated for another 24 hours at 37°C. The cells were then detached using accutase, spun down and resuspended in PBS before analysis on the flow cytometer.
Instrument	BD LSRFortessa
Software	LSR Fortessa cell analyzer (BD Biosciences) was used in data aquisition. FlowJo v10.6 (FlowJo LLC) was used in the analysis of the flow cytometry data.
Cell population abundance	Samples were not sorted. At least 10^4 cells were analyzed per condition.
Gating strategy	Dead cells showing high DAPI signal and multiplets with large forward scattering were removed through gating. Untransfected cells that showed neither green nor red fluorescence were then removed in a second step. Quantification of Cre positive cells was done on the remaining cell population.

☒ Tick this box to confirm that a figure exemplifying the gating strategy is provided in the Supplementary Information.